Nanomechanics of pectin-linked β-lactoglobulin nanofibril bundles

Simon M. Loveday[†,§,*], *A. Patrick Gunning*[‡]

[†] AgResearch Limited, Grasslands Research Centre, Tennent Drive, Private Bag 11008, Palmerston North, 4442, New Zealand.

Formerly: Massey Institute of Food Science & Technology, Massey University, Palmerston North 4442, New Zealand.

[§] Riddet Institute Centre of Research Excellence, Massey University, Palmerston North 4442, New Zealand.

[‡] Quadram Institute Bioscience, Norwich Research Park, Norwich, Norfolk, NR4 7UA, UK

The final version of the article appears as Loveday and Gunning, Biomacromolecules 2018, 19, 2834−2840. DOI: 10.1021/acs.biomac.8b00408

KEYWORDS:
Protein nanofibril, pectin, atomic force microscopy, persistence length, force spectroscopy, worm-like chain

ABSTRACT

Nanofibrils of β-lactoglobulin can be assembled into bundles by site-specific noncovalent crosslinking with high-methoxyl pectin (Hettiarachchi et al. Soft Matter 12(756) 2016). Here we characterised the nanomechanical properties of bundles using atomic force microscopy and force spectroscopy. Bundles had Gaussian cross-sections and mean height of 17.4 ± 1.4 nm. Persistence lengths were calculated using image analysis with the mean-squared end-to-end model. The relationship between persistence length and the thickness had exponents of 1.77 to 2.3, which is consistent with previous reports for other fibril types. In force spectroscopy experiments the bundles stretched in a qualitatively different manner to fibrils, and some of the force curves were consistent with peeling fibrils away from bundles. The flexibility of pectin-linked nanofibril bundles is likely to be tuneable by modulating the stiffness and length of fibrils and the ratio of pectin to fibrils, giving rise to a wide range of structures and functionalities.

Introduction

Amyloid-like protein nanofibrils consist of proteins or peptides assembled via β-sheet stacking to form long thin structures capable of intertwining into physical entanglement networks. Fibrillar structures of this kind are seen in nature, both in certain pathologies (e.g. amyloidosis[1]) and non-pathological contexts (e.g. human melanosome biogenesis[2], reinforcement of silk moth egg shells[3]). They form hydrogels at lower concentration than other forms of protein aggregate[4, 5], and have potential applications ranging from tissue scaffolds to filters and biosensors[6].

Many proteins can be induced to assemble into amyloid-like fibrils *in vitro.* The bovine milk protein β-lactoglobulin (β-lg) assembles particularly rapidly at low pH and temperature > 75 ºC; its low cost and ready availability make it an attractive material for fibril-based industrial applications. β-Lg nanofibrils have morphology that depends on solution conditions: at very low ionic strength or high temperature[7] they assemble as long semiflexible structures (persistence length, λ_p the same order of magnitude as contour length), whereas they are shorter and more flexible, with 'worm-like' characteristics (λ_p << contour length) when assembly occurs at ionic strength above ~30 mM[8, 9]. Recent evidence suggests that worm-like fibrils can also form at low ionic strength and high protein concentration[10, 11].

Individual β-lg nanofibrils are 4-8 nm thick[12, 13] and up to 10 μm long[7], and they can be crosslinked via noncovalent site-specific interactions with certain pectins to form tapes or bundles[14, 15]. The pectin structural features that give rise to bundle formation and the solution conditions under which it occurs have been extensively studied[16]. However little is known about the nanomechanical properties of pectin-linked fibril bundles or the forces holding them together.

Atomic force microscopy (AFM) is a unique class of techniques in which samples are probed with a fine tip that is held, pushed into, or moved over the sample surface[17-20]. It can produce three-dimensional images but can also probe mechanical properties by pulling apart nanostructures (force spectroscopy). Here we used AFM to report on the morphology of pectin-linked fibril bundles, and examine nanomechanical properties using image analysis and force spectroscopy.

Experimental

Materials.

β-lg was isolated from whey protein isolate 8855 (Fonterra Cooperative Ltd., Auckland, New Zealand) using a salt precipitation method[21]. It consisted of 97 % w/w protein and was a mixture of β-lg variants A and B. Citrus pectin with a degree of methoxylation ≥ 85% (P9561) was purchased from Sigma Aldrich (Dorset, England). Previous analysis of this pectin revealed a galacturonic acid content of 88.5 % w/w (dry basis) and average degree of methoxylation of 86 ± 2 %[14]. All other chemicals were of analytical or reagent grade.

Assembly of fibrils and bundles.

Semiflexible fibrils were made by heating a 1 % w/v solution of acidified (pH 2) β-lg at 90 °C with orbital shaking (300 rpm) for 15 hours in a Thermomixer C (Eppendorf AG, Hamburg, Germany). Wormlike fibrils were made under the same conditions except with 100 mM NaCl added prior to heating.
Pectin-linked nanofibril bundles were prepared as previously described[14]. Fibril solutions were diluted and mixed at ambient temperature with pectin solutions to give a protein concentration of 1 mg.mL^{-1} and pectin concentration of 0.05 mg.mL^{-1}.

Atomic Force Microscopy.

The atomic force microscope (AFM) used in this study was MFP-3D BIO (Oxford Instruments Company, Asylum Research, Santa Barbara, California, USA). The AFM tips used for force spectroscopy were silicon nitride contact mode cantilevers (PNP-TR, Nanoworld AG, Neuchâtel, Switzerland) and for imaging the tips were silicon AC mode cantilevers (OMCL-AC160TS-R3, Olympus Corporation, Japan).

Sample preparation

The fibril samples were diluted 1:9 v/v with Milli-Q water and incubated onto two freshly cleaved substrates for minimum of 60 seconds and then the substrates rinsed with pure water to avoid salt crystallisation on the substrates. Reasons for using two substrates: Highly orientated pyrolytic graphite (HOPG) attaches the fibrils due to its hydrophobicity. Mica was pre-coated with poly-l-lysine to make it fully positively charged to attach the fibrils hence the water rinsing didn't remove the fibrils. As previously mentioned imaging was carried out in air in AC mode that gives multiple data as pointed out in the result section, topography and phase images. The adjustment of the cantilever's phase oscillation is the transfer of energy from the tip as it interacts with the sample that it raster scans and it generates more contrast as the tip hits different regions of the sample due to variations in sample modulus.

Force spectroscopy

The force spectroscopy measurement of the fibrils was created in aqueous liquid (PBS buffer pH 7.4) with the samples attached to HOPG. The experimental data were captured in 'force-volume' (FV) mode at a rate of 2 μm s^{-1} in the Z direction (perpendicular to sample surface) and at a scan rate of 1 Hz and a load force of 400 pN (pixel density of 32 x 32 which collects 1024 force-distance curves). The FV mode starts the AFM tip above the sample surface, approaches the surface until it reaches the loading force of 400 pN it then dwells for 1 s to attach the fibril/bundle to the tip. The tip then retracts away from the surface and stretches the attached fibril/bundle. The spring constant, *k*, of

the cantilevers was determined by fitting the thermal noise spectra in the Get Real™ version, yielding values of 81.32 pN.nm^{-1}.

Data Analysis.

AFM data were analysed with Asylum Research AFM software v14.23.153 (Asylum Research, Santa Barbara, California, USA), running in IGOR Pro v6.34A (Wavemetrics Inc., Oregon, USA). Nonlinear force curves were fitted with the worm-like chain model[22] (eq 1) using the Asylum WLC tool. In this equation F is force, λ_p is persistence length, k_B is the Boltzmann constant, T is temperature, L_c is contour length and x is extension.

$$\frac{F\lambda_p}{k_B T} = \frac{1}{4}\left(1 - \frac{x}{L_c}\right)^{-2} - \frac{1}{4} + \frac{x}{L_c} \qquad (1.)$$

Phase image montages were constructed in Adobe Photoshop CC 2017 (Adobe Inc.) using images exported from Asylum software as tiff files.

For cross-sectioning, height images were flattened in Asylum software with flatten order 3, then sections were drawn in line or freehand mode (for bundles and fibrils respectively) and raw data were exported to Excel for Mac v16.10 (Microsoft Corporation, Redmond, Washington, USA). Bundle cross sections were fitted with a Gaussian equation (eq 2) using the Igor 'quick fit' function, and the indefinite integral of this function (eq 3) gave the area under the curve (AUC).

$$y = y_0 + Aexp\left\{-\left(\frac{z - z_0}{2w^2}\right)^2\right\} \qquad (2.)$$

$$AUC = \int_{-\infty}^{\infty} y = Aw \cdot \sqrt{2\pi} \qquad (3.)$$

In these equations y is height, y_0 is baseline height, A is amplitude (maximum height), z is position along the cross-section, z_0 is the position where $y = A$, and w is a measure of the width of the distribution.

Fibril cross sections were drawn with freehand mode by repeatedly crossing a given fibril (Fig S1), which gave 5 to 14 peaks. Baselines were set by subtracting the average of the 10 lowest height measurements, and peak heights for a given fibril were averaged. Height measurements of 10 semiflexible fibrils were obtained in this way.

Fibril and bundle persistence lengths were calculated by image analysis using Fiber-App v2.1[23]. The mean-squared end-to-end model (eq 4) provided consistently good fits.

$$\langle R^2 \rangle = 4\lambda_p\left[l - 2\lambda_p\left(1 - e^{-1/2\lambda_p}\right)\right] \qquad (4.)$$

In eq 4 R is the direct distance between a pair of segments along a contour of arc length l, and λ_p is the persistence length. Relationships between λ_p and other variables were fitted with nonlinear regression in R v3.4.3[24].

Results and Discussion

Nanofibril bundles were very heterogenous; bundles of different thicknesses converged, diverged and overlapped. A skein of nanofibril bundles is shown in Figure 1, which is a montage of several overlapping AFM phase signal images. This structural complexity is similar to the cryo-electron microscopy images reported previously [14], and provides cross-validation that no major artefacts were present. The air-drying process could potentially have caused lateral contraction of bundles due to capillary forces, and this was checked by imaging bundles fibrils in phosphate-buffered saline, i.e. in a fully hydrated state (Fig S2). In one case the cross-section was a flattened peak, but in other cases the cross-

section was sharp or Gaussian, indicating that drying did not substantially modify the morphology of bundles.

Figure 1. Phase image montage of pectin-nanofibril bundles.

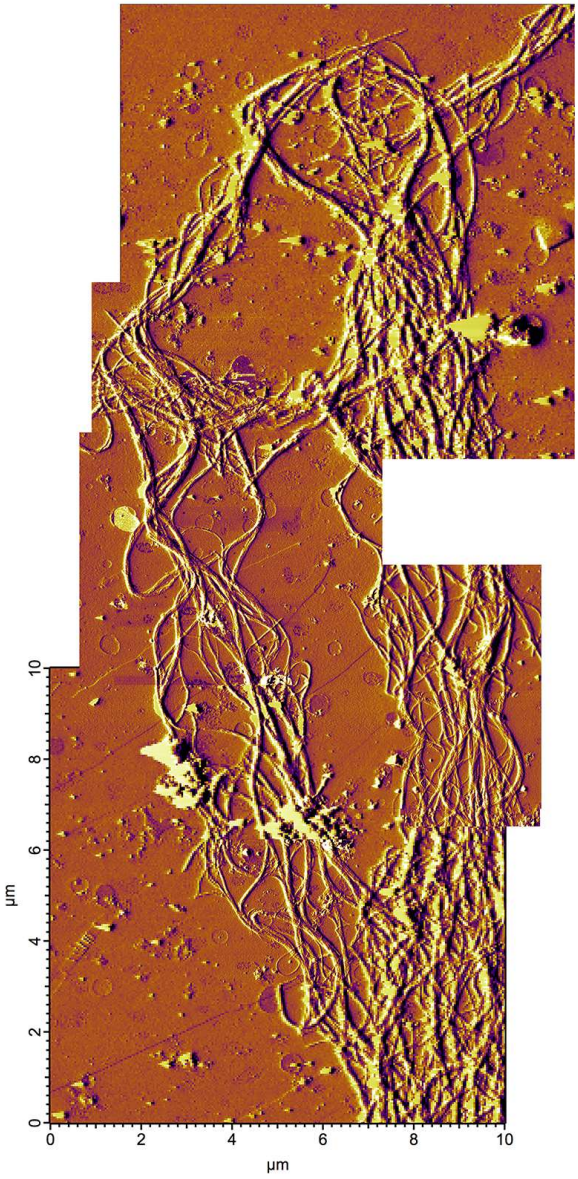

Cross-sectional profiles of fibril-pectin bundles were obtained from AFM height data, and Figure 2 shows representative examples. Heights varied from 4.8 nm (probably a single multi-filament fibril) to nearly 50 nm, with a mean of 17.4 ± 1.4 nm. Perpendicular cross sections of pectin-fibril bundles were highly Gaussian in almost all cases, as illustrated by excellent fits with Eq 1 in Figure 2.

Figure 2. Top: AFM phase image of pectin-bonded β-lactoglobulin protein nanofibril bundles. Bottom: cross-sections obtained at locations A, B, C and D are plotted below (points) and fitted with eq 2 (lines).

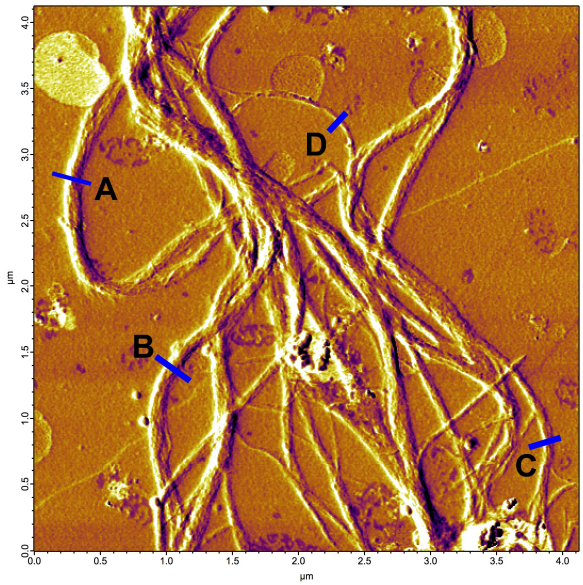

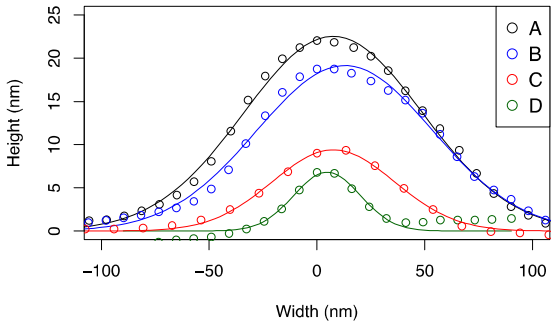

Because of limited resolution it was not possible to directly count the number of fibrils *n* within each bundle; three alternative approaches were used. Approach 1 was to calculate the indefinite integral of Eq 1, i.e. the area under the curve (AUC), which is approximately proportional to the number of fibrils in a bundle. Approach 2 was to use the fitted bundle height, A in eq 2, as a measure of bundle size that is indirectly related to the number of fibrils.

Approach 3 assumed that fibrils within a bundle were of uniform circular cross-section with diameter *d*, and were close-packed in a pyramidal arrangement comprising *N* layers of fibrils (see **Supporting Information**). The height of the bundle at the centre of the cross section is denoted *h*, and was approximated with the fitted value, *A*. The equation relating *h* to *d* and *N* is derived in **Supporting Information** Fig S3 and shown in eq 4. Solving for *N* gives eq 6, and the number of fibrils in a close-packed bundle (*n*) can be derived from *N* via eq 6.

$$h = d + (N-1)\cdot\frac{d}{2}\left(1+2\sqrt{1-\frac{\sqrt{3}}{2}}\right) \qquad (5.)$$

$$N = \frac{2(h-d)}{d\left(1+2\sqrt{1-\frac{\sqrt{3}}{2}}\right)} + 1 \qquad (6.)$$

$$n = \sum_{i=0}^{i=N-1} N - i \qquad (7.)$$

The average height of individual fibrils (*d*) was estimated by sectioning height images of individual fibrils without pectin (see **Supporting Information**). Individual fibrils had heights of 1.63 ± 0.11 nm (n = 6) or 5.26 ± 0.21 nm (n = 4), probably representing single filaments and multi-filament fibrils respectively[25]. Solutions of β-lg nanofibrils made in this way invariably contain a mixture of individual filaments and fibrils of varying thicknesses, and the pectin-linked bundles are likely to be comprised of similarly mixed strands. For the purposes of estimating the number of fibrils in bundles (see below) the individual cross-section heights were pooled to give a mean height of 3.08 ± 0.60 nm (n=10).

Data from each of the 3 approaches are plotted in Figure 3, and Table 1 shows the results of nonlinear regression of these data using the fit equation $y = x^a + b$ with λ_p^{-1} weighting.

Figure 3. A: relationship between persistence length and area (Approach 1); B: relationship between persistence length and fitted bundle height (Approach 2); C: relationship between persistence length and estimated number of fibrils (Approach 3).

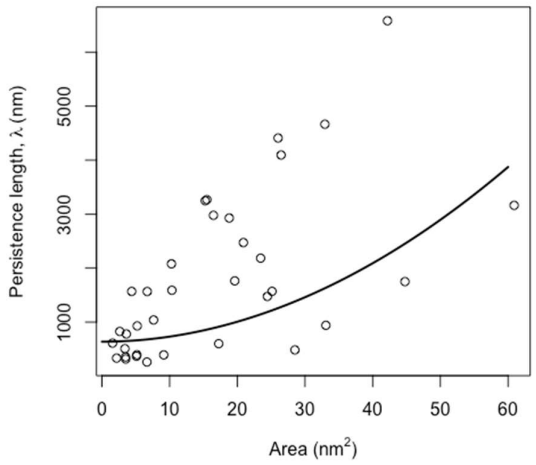

A:

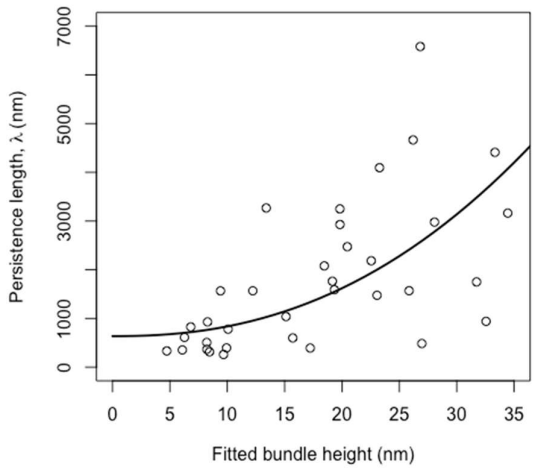

B:

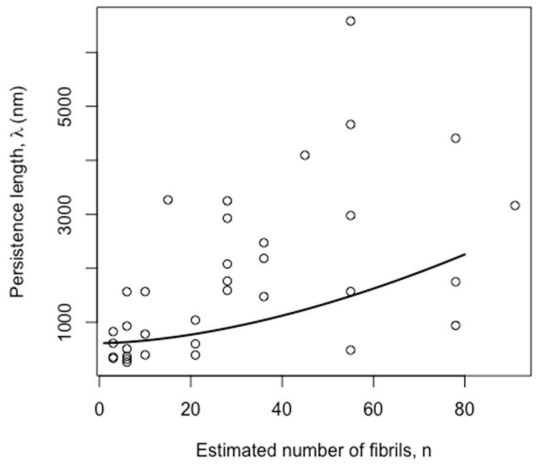

C:

Table 1. Nonlinear regression results showing the relationship between persistence length and various measures of the number of fibrils in each bundle. *** $p < 0.001$, ** $p < 0.01$

x variable	y variable	exponent, *a*	intercept, *b*	RSE[a]
area under the curve	λ_p	1.97 ± 0.08***	636.4 ± 145.0***	27.44
fitted bundle height	λ_p	2.30 ± 0.06***	691.1 ± 203.5**	275.3
estimated number of fibrils	λ_p	1.68 ± 0.08***	611 ± 151***	27.78

a: residual standard error

The fit parameters for nonlinear regression lines were highly significant in all cases, and residual standard errors were low. The three approaches for testing the relationship between fibril size and λ gave exponents close to 2, which is in agreement with the findings of Wang, et al. [26] for sickle cell haemoglobin fibres, and with the model for β-lg nanofibril flexibility proposed by Usov and Mezzenga [27]. Nanomechanical relationships observed in related protein fibre systems appear to apply equally to pectin-bonded β-lg nanofibril bundles, despite thicknesses up to an order of magnitude larger. Although it was not possible to directly count the number of fibrils comprising bundles, we estimated that bundles contained up to 78 fibrils, but mostly between 21 and 36 fibrils (6-8 layers).

In addition to static observations of bundle morphology, force spectroscopy experiments were conducted on semiflexible fibrils and pectin-fibril bundles. Wormlike β-lg nanofibrils that assembled during heating with 100 mM NaCl were also probed, since no force spectroscopy data for this system have been reported before. The morphology of wormlike fibrils is shown in **Supporting Information** Fig S4. Figure 4 shows representative stretches for semiflexible fibrils, wormlike fibrils and pectin-fibril bundles, with single or multiple 'hitches', i.e. negative force peaks.

Figure 4. Example stretches from single-molecule force spectroscopy experiments. Stretches are vertically shifted for clarity.

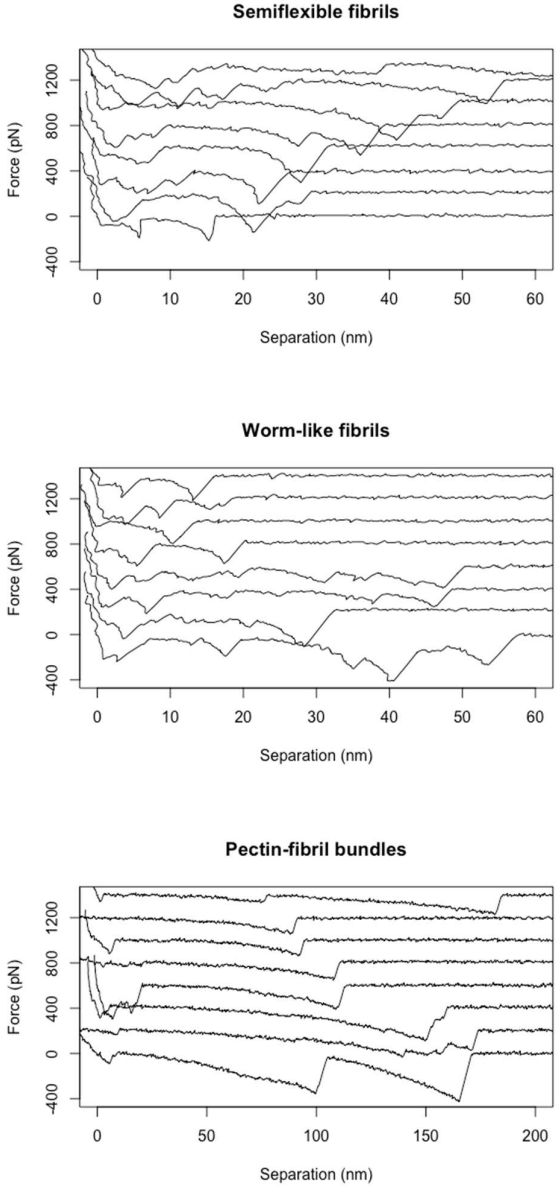

There are clear qualitative differences between stretches from pectin-fibril bundles and those from individual fibrils (wormlike or semiflexible). The rupture length is much larger for bundles, and stretches with low rupture force are common. Nonlinear stretches were observed with bundles and both fibril types, and they were fitted with the worm-like chain (WLC) model using Asylum software. The WLC equation was a good fit to nonlinear stretches, but it produced mostly sub-nanometre persistence lengths, which is not consistent with the dimensions of the structures being stretched. The software also provided direct model-independent measurements of rupture length and rupture force; these parameters are plotted in Figure 5.

Figure 5. Rupture parameters obtained by fitting single molecule force spectroscopy data with the worm-like chain model.

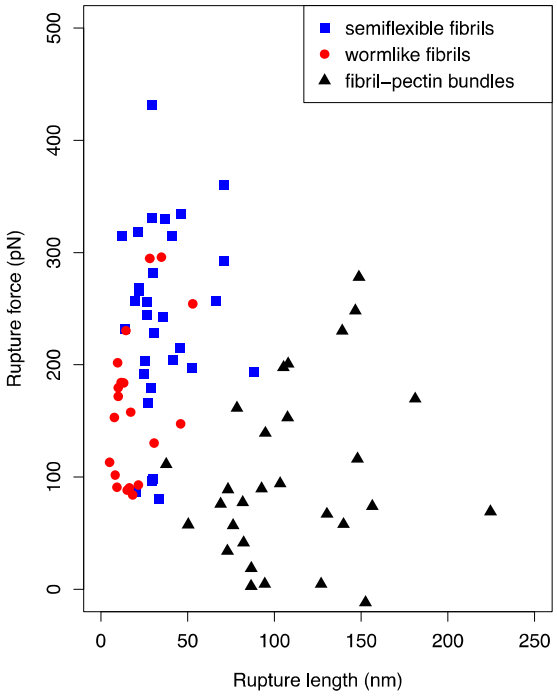

Quantitative stretch parameters revealed that fibril-pectin bundles were stretched to longer lengths before the contact between AFM tip and the sample was ruptured, and there was a wide spread of rupture lengths. By contrast individual fibrils ruptured at shorter lengths and exhibited a narrow range of rupture lengths. Higher rupture forces were observed for individual fibrils, especially semiflexible fibrils. Wormlike fibrils generally ruptured at lower force and shorter length than semiflexible fibrils, though there were some exceptions.

Force curves from pectin-fibril bundles occasionally showed ‘staircase’ or ‘sawtooth’ patterns, exhibiting several oblique force plateaux in succession (Figure 6). These were not seen for individual fibrils of either type, although they have been observed before with native β-lg and β-lg nanofibrils[28, 29], as well as amyloid-β nanofibrils[30] and nanofibrillar algal proteins[31, 32].

Figure 6. Examples of 'staircase' or 'sawtooth' stretching patterns observed with pectin-nanofibril bundles.

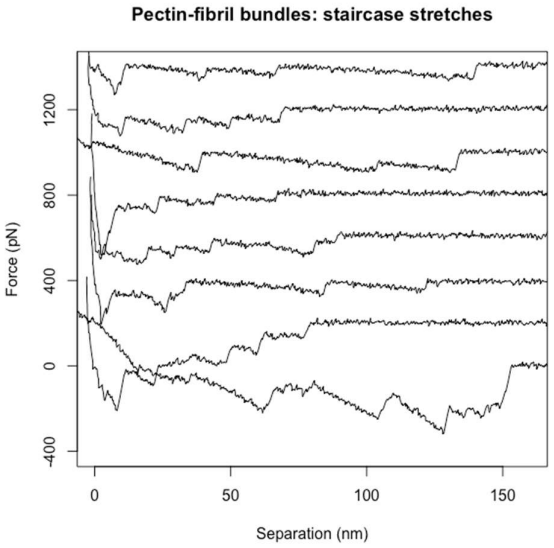

Staircase patterns seen with pectin-fibril bundles were quite heterogeneous in terms of the spacing, depth and number of ruptures. In native β-lg staircase patterns were attributed to simultaneous axial stretching of a protein and peeling off a substrate[28]. The secondary structure of β-lg is completely disrupted by heating during fibril formation[33], so that cannot be the explanation here. Alternatively, the hitches may be due to the rupture of pectin-fibril linkages holding the bundles together. Structural modelling of the pectin on the basis of selective hydrolysis[14] indicates that pectin chains are approximately 192 residues long with the majority of non-methylesterified galacturonic acid in 2 or 3 blocks. The spacing between blocks is in the order of 90 residues, and if each residue is ~4.4 Å[34] this would give a hypothetical average hitch spacing of ~40 nm. This is consistent with the pattern of hitches in Figure 6, and the predominantly small rupture forces are in keeping with the weak noncovalent pectin-fibril interactions[14] holding bundles together.

Conclusions

Pectin-linked β-lg nanofibril bundles are a new type of hierarchical mesostructure with unexplored potential. We have shown that scaling laws between thickness and flexibility that were established with much thinner protein fibrils are also applicable to this system. The pectin-fibril interactions that crosslink fibrils into bundles are relatively weak, and this may explain modest persistence lengths, in that weak crosslinks allow fibrils to slide within bundles when a bundle flexes. The flexibility of nanofibril bundles is likely to be tuneable by modulating the stiffness and length of fibrils and the ratio of pectin to fibrils, giving rise to a wide range of structures and functionalities.

Supporting Information

The following files are available free of charge.

'Supporting Info | Loveday and Gunning | Biomacromolecules.pdf': Examples of fibril cross-sectioning, bundle appearance in buffer, derivation of eq 5-7, AFM images of worm-like fibrils: Further AFM images of fibrils

AUTHOR INFORMATION

Corresponding Author

* Email: s.loveday@massey.ac.nz. Tel: +64 6 951 7259

Author Contributions

The manuscript was written through contributions of all authors. All authors have given approval to the final version of the manuscript.

Funding Sources

This work was supported by a UK BBSRC Other Countries Partnering Award and the Riddet Institute, a national Centre of Research Excellence funded by the New Zealand Tertiary Education Commission and hosted at Massey University.

Acknowledgment

SML thanks Prof. Alan Mackie, University of Leeds, for facilitating a sabbatical visit to Norwich.

Abbreviations

A	amplitude parameter in Gaussian fit equation
AFM	atomic force microscopy
AUC	area under the curve
β-lg	β-lactoglobulin
F	force
d	mean diameter of fibrils
h	bundle height
k_B	Boltzmann constant
k	AFM cantilever spring constant
L_c	contour length
λ_p	persistence length
n	number of fibrils in a bundle
N	number of fibril layers in a bundle
r	radius of circular fibril cross-section

T temperature

w width parameter in Gaussian fit equation

x extension in force spectroscopy experiments

y height

y_0 baseline height

z position along fibril/bundle cross-section

z_0 position at which $y = A$

References

1. Knowles, T. P. J.; Buehler, M. J., Nanomechanics of functional and pathological amyloid materials. *Nature Nanotechnology* **2011,** 6, (8), 469-479.
2. Berson, J. F.; Theos, A. C.; Harper, D. C.; Tenza, D.; Raposo, G.; Marks, M. S., Proprotein convertase cleavage liberates a fibrillogenic fragment of a resident glycoprotein to initiate melanosome biogenesis. *Journal of Cell Biology* **2003,** 161, (3), 521-533.
3. Iconomidou, V. A.; Hamodrakas, S. J., Natural protective amyloids. *Current Protein and Peptide Science* **2008,** 9, (3), 291-309.
4. Kavanagh, G. M.; Clark, A. H.; Ross-Murphy, S. B., Heat-induced gelation of globular proteins: 4. Gelation kinetics of low pH β-lactoglobulin gels. *Langmuir* **2000,** 16, (24), 9584-9594.
5. Loveday, S. M.; Rao, M. A.; Creamer, L. K.; Singh, H., Factors affecting rheological characteristics of fibril gels: The case of β-lactoglobulin and α-lactalbumin. *Journal of Food Science* **2009,** 74, (3), R47-R55.
6. Wei, G.; Su, Z. Q.; Reynolds, N. P.; Arosio, P.; Hamley, I. W.; Gazit, E.; Mezzenga, R., Self-assembling peptide and protein amyloids: from structure to tailored function in nanotechnology. *Chemical Society Reviews* **2017,** 46, (15), 4661-4708.
7. Loveday, S. M.; Wang, X. L.; Rao, M. A.; Anema, S. G.; Singh, H., β-Lactoglobulin nanofibrils: Effect of temperature on fibril formation kinetics, fibril morphology and the rheological properties of fibril dispersions. *Food Hydrocolloids* **2012,** 27, (1), 242-249.
8. Aymard, P.; Nicolai, T.; Durand, D.; Clark, A., Static and dynamic scattering of β-lactoglobulin aggregates formed after heat-induced denaturation at pH 2. *Macromolecules* **1999,** 32, (8), 2542-2552.
9. Loveday, S. M.; Wang, X. L.; Rao, M. A.; Anema, S. G.; Creamer, L. K.; Singh, H., Tuning the properties of β-lactoglobulin nanofibrils with pH, NaCl and $CaCl_2$. *International Dairy Journal* **2010,** 20, 571-579.
10. Miti, T.; Mulaj, M.; Schmit, J. D.; Muschol, M., Stable, metastable, and kinetically trapped amyloid aggregate phases. *Biomacromolecules* **2015,** 16, (1), 326-335.
11. Ye, X.; Hedenqvist, M. S.; Langton, M.; Lendel, C., On the role of peptide hydrolysis for fibrillation kinetics and amyloid fibril morphology. *RSC Advances* **2018,** 8, (13), 6915-6924.
12. Adamcik, J.; Mezzenga, R., Adjustable twisting periodic pitch of amyloid fibrils. *Soft Matter* **2011,** 7, (11), 5437-5443.

13. Bolisetty, S.; Adamcik, J.; Mezzenga, R., Snapshots of fibrillation and aggregation kinetics in multistranded amyloid b-lactoglobulin fibrils. *Soft Matter* **2011,** 7, (2), 493-499.
14. Hettiarachchi, C. A.; Melton, L. D.; McGillivray, D. J.; Loveday, S. M.; Gerrard, J. A.; Williams, M. A. K., β-Lactoglobulin nanofibrils can be assembled into nanotapes via site-specific interactions with pectin. *Soft Matter* **2016**.
15. Loveday, S. M.; Anema, S. G.; Singh, H., β-Lactoglobulin nanofibrils: The long and the short of it. *International Dairy Journal* **2017,** 67, 35-45.
16. Hettiarachchi, C. A.; Melton, L. D.; Williams, M. A. K.; McGillivray, D. J.; Gerrard, J. A.; Loveday, S. M., Morphology of complexes formed between β-lactoglobulin nanofibrils and pectins is influenced by the pH and structural characteristics of the pectins. *Biopolymers* **2016,** 105, 819-831.
17. Morris, V. J.; Woodward, N. C.; Gunning, A. P., Atomic force microscopy as a nanoscience tool in rational food design. *Journal of the Science of Food and Agriculture* **2011,** 91, (12), 2117-2125.
18. Adamcik, J.; Mezzenga, R., Study of amyloid fibrils via atomic force microscopy. *Current Opinion in Colloid and Interface Science* **2012**.
19. Gunning, A. P.; Grant, C. A., Scratching the surface: An overview of scanning probe microscopy (SPM). *InFocus | The Proceedings of the Royal Microscopical Society* **2016,** 42, 56-69.
20. Lee, W.; Lee, H.; Lee, G.; Yoon, D. S., Advances in AFM imaging applications for characterizing the biophysical properties of amyloid fibrils. In *Exploring new findings on amyloidosis*, Fernandez-Escamilla, A. M., Ed. InTech: 2016.
21. Dave, A. C.; Loveday, S. M.; Anema, S. G.; Loo, T. S.; Norris, G. E.; Jameson, G. B.; Singh, H., β-Lactoglobulin self-assembly: Structural changes in early stages and disulfide bonding in fibrils. *Journal of Agricultural and Food Chemistry* **2013,** 61, 7817-7828.
22. Marko, J. F.; Siggia, E. D., Stretching DNA. *Macromolecules* **1995,** 28, (26), 8759-8770.
23. Usov, I.; Mezzenga, R., FiberApp: An open-source software for tracking and analyzing polymers, filaments, biomacromolecules, and fibrous objects. *Macromolecules* **2015,** 48, (5), 1269-1280.
24. R Core Team. R: A language and environment for statistical computing. http://www.R-project.org/ accessed 5 May 2015
25. Adamcik, J.; Jung, J. M.; Flakowski, J.; De Los Rios, P.; Dietler, G.; Mezzenga, R., Understanding amyloid aggregation by statistical analysis of atomic force microscopy images. *Nature Nanotechnology* **2010,** 5, (6), 423-428.
26. Wang, J. C.; Turner, M. S.; Agarwal, G.; Kwong, S.; Josephs, R.; Ferrone, F. A.; Briehl, R. W., Micromechanics of isolated sickle cell hemoglobin fibers: Bending moduli and persistence lengths. *Journal of Molecular Biology* **2002,** 315, (4), 601-612.
27. Usov, I.; Mezzenga, R., Correlation between Nanomechanics and Polymorphic Conformations in Amyloid Fibrils. *ACS Nano* **2014,** 8, (11), 11035-11041.
28. Dunstan, D. E.; Hamilton-Brown, P.; Asimakis, P.; Ducker, W.; Bertolini, J., Shear-induced structure and mechanics of β-lactoglobulin amyloid fibrils. *Soft Matter* **2009,** 5, (24), 5020-5028.
29. Touhami, A.; Dutcher, J. R., pH-induced changes in adsorbed β-lactoglobulin molecules measured using atomic force microscopy. *Soft Matter* **2009,** 5, (1), 220-227.
30. Kellermayer, M. S. Z.; Grama, L.; Karsai, Á.; Nagy, A.; Kahn, A.; Datki, Z. L.; Penke, B., Reversible mechanical unzipping of amyloid β-fibrils. *Journal of Biological Chemistry* **2005,** 280, (9), 8464-8470.

31. Mostaert, A. S.; Jarvis, S. P., Beneficial characteristics of mechanically functional amyloid fibrils evolutionarily preserved in natural adhesives. *Nanotechnology* **2007,** 18, (4).
32. Mostaert, A. S.; Higgins, M. J.; Fukuma, T.; Rindi, F.; Jarvis, S. P., Nanoscale mechanical characterisation of amyloid fibrils discovered in a natural adhesive. *Journal of Biological Physics* **2006,** 32, (5), 393-401.
33. Dave, A. C.; Loveday, S. M.; Anema, S. G.; Jameson, G. B.; Singh, H., Modulating β-lactoglobulin Nanofibril Self-Assembly at pH 2 Using Glycerol and Sorbitol. *Biomacromolecules* **2014,** 15, (1), 95-103.
34. Cros, S.; du Penhoat, C. H.; Bouchemal, N.; Ohassan, H.; Imberty, A.; Pérez, S., Solution conformation of a pectin fragment disaccharide using molecular modelling and nuclear magnetic resonance. *International Journal of Biological Macromolecules* **1992,** 14, (6), 313-320.

Table of Contents graphic

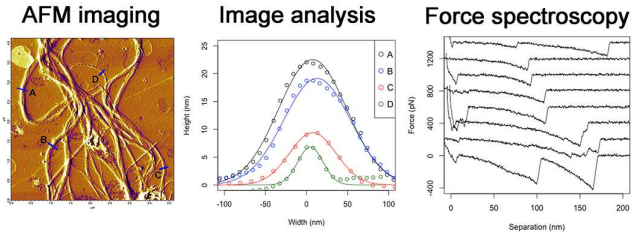

Loveday and Gunning, Biomacromolecules 2018, 19, 2834−2840. DOI: 10.1021/acs.biomac.8b00408

Supplementary Material

Nanomechanics of pectin-linked whey protein nanofibril bundles

Simon M. Loveday[†,§,*]*, A. Patrick Gunning*[‡]

[†] AgResearch Limited, Grasslands Research Centre, Tennent Drive, Private Bag 11008, Palmerston North, 4442, New Zealand.

Formerly: Massey Institute of Food Science & Technology, Massey University, Palmerston North 4442, New Zealand.

[§] Riddet Institute Centre of Research Excellence, Massey University, Palmerston North 4442, New Zealand.

[‡] Quadram Institute Bioscience, Norwich Research Park, Norwich, Norfolk, NR4 7UA, UK

Fig S1: Cross-sectioning of individual fibrils imaged in air.

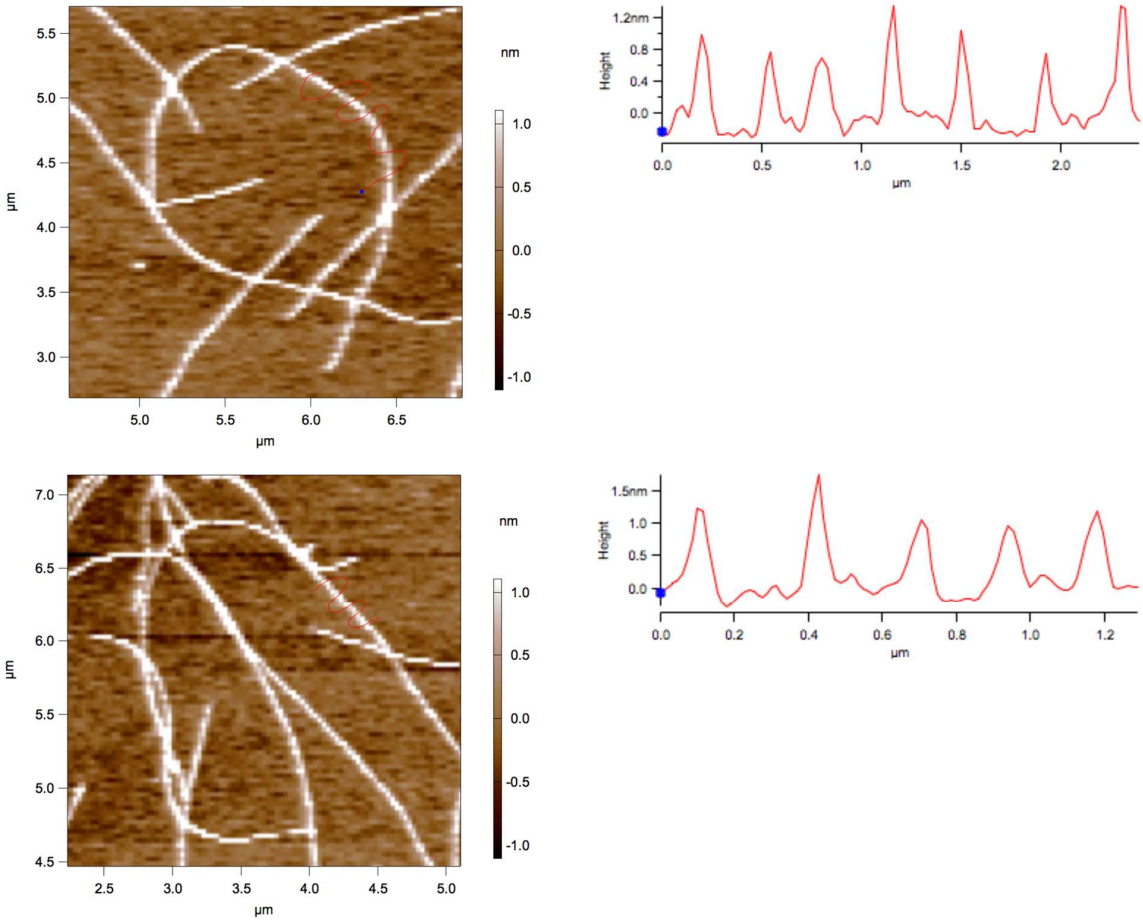

Fig S2: Cross-sections of pectin-nanofibril bundles imaged in PBS buffer.

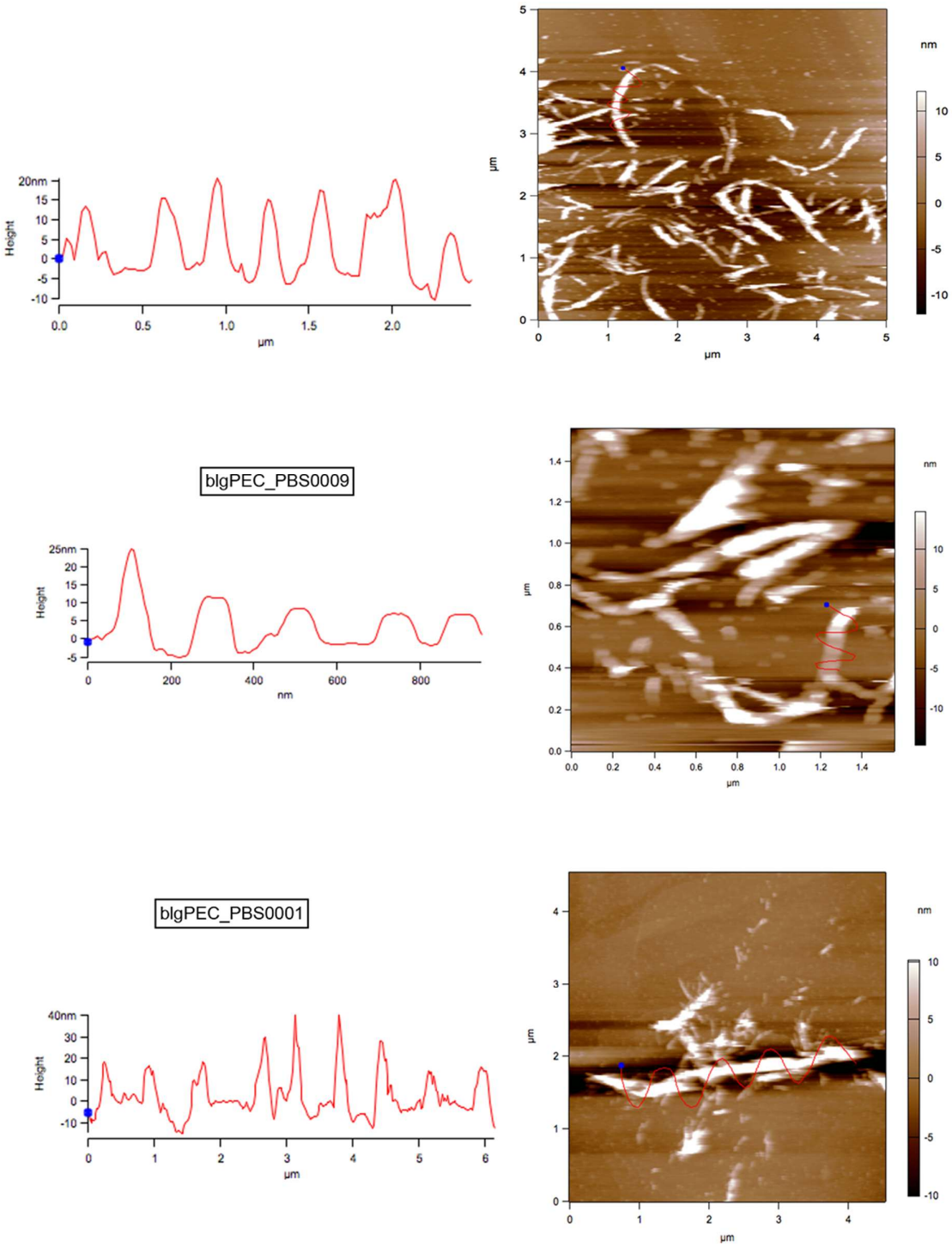

Calculating overlap height between layers of hexagonal close-packed fibrils, where *d* is fibril diameter and *r/2* is fibril cross-sectional radius:

Fig S3A.

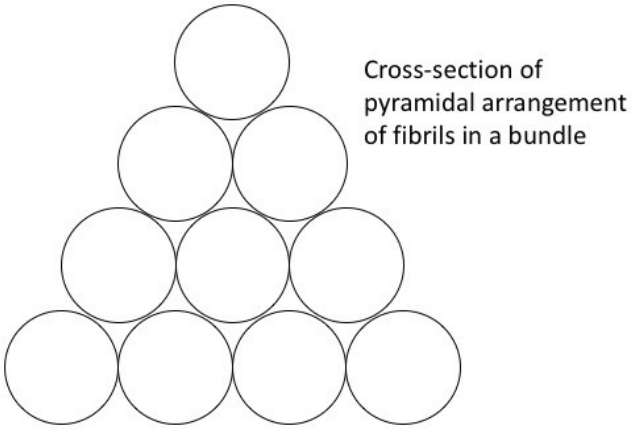

Fig S3B.

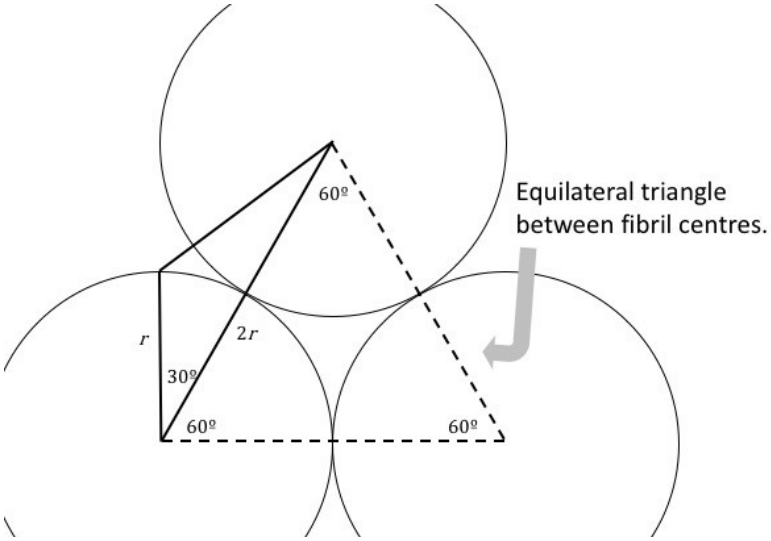

Fig S3C.

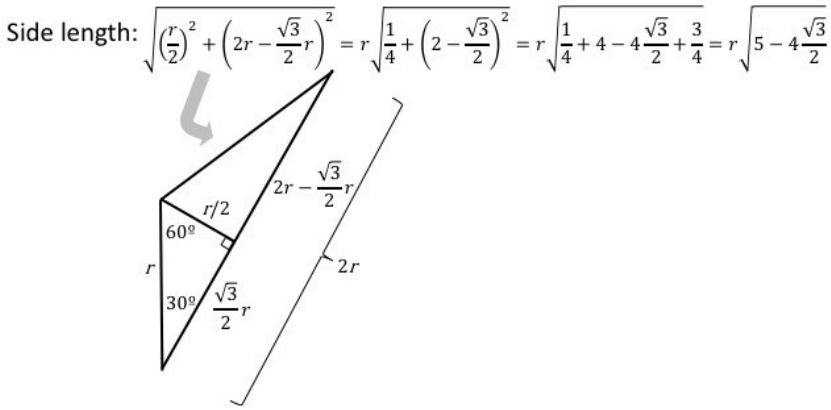

Fig S3D.

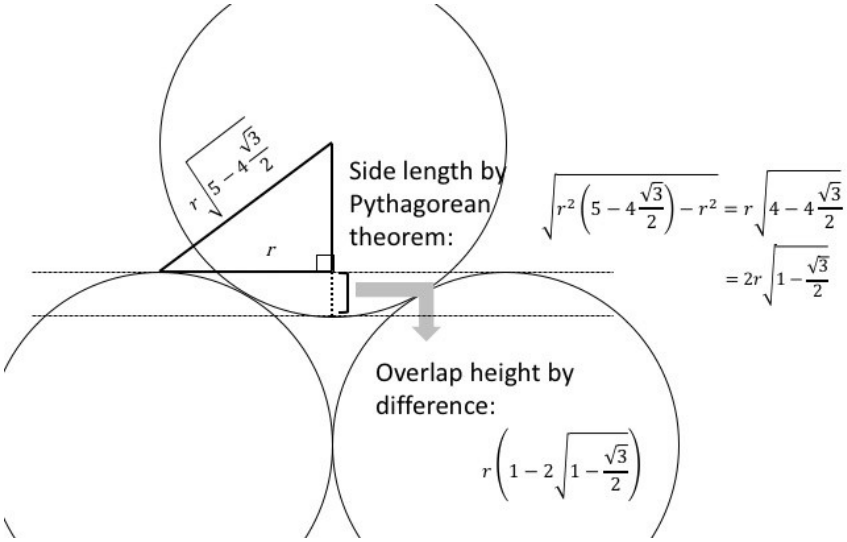

Overlap height is

$$r\left(1-2\sqrt{1-\frac{\sqrt{3}}{2}}\right)=0.2679\times r$$

Effective height of an overlapped layer:

$$2r - r\left(1 - 2\sqrt{1 - \frac{\sqrt{3}}{2}}\right) = r\left(1 + 2\sqrt{1 - \frac{\sqrt{3}}{2}}\right)$$

Effective height: reparameterising with $r = d/2$:

$$\frac{d}{2}\left(1 + 2\sqrt{1 - \frac{\sqrt{3}}{2}}\right) = 0.866d$$

Total height h of a cross-section of N layers of pyramidally-arranged fibrils:

$$h = d + (N - 1) \cdot \frac{d}{2}\left(1 + 2\sqrt{1 - \frac{\sqrt{3}}{2}}\right)$$

Solving for N:

$$(N - 1)\left(1 + 2\sqrt{1 - \frac{\sqrt{3}}{2}}\right) = \frac{2(h - d)}{d}$$

$$N = \frac{2(h - d)}{d\left(1 + 2\sqrt{1 - \frac{\sqrt{3}}{2}}\right)} + 1$$

Fig S4: AFM images illustrating the morphology of wormlike fibrils.

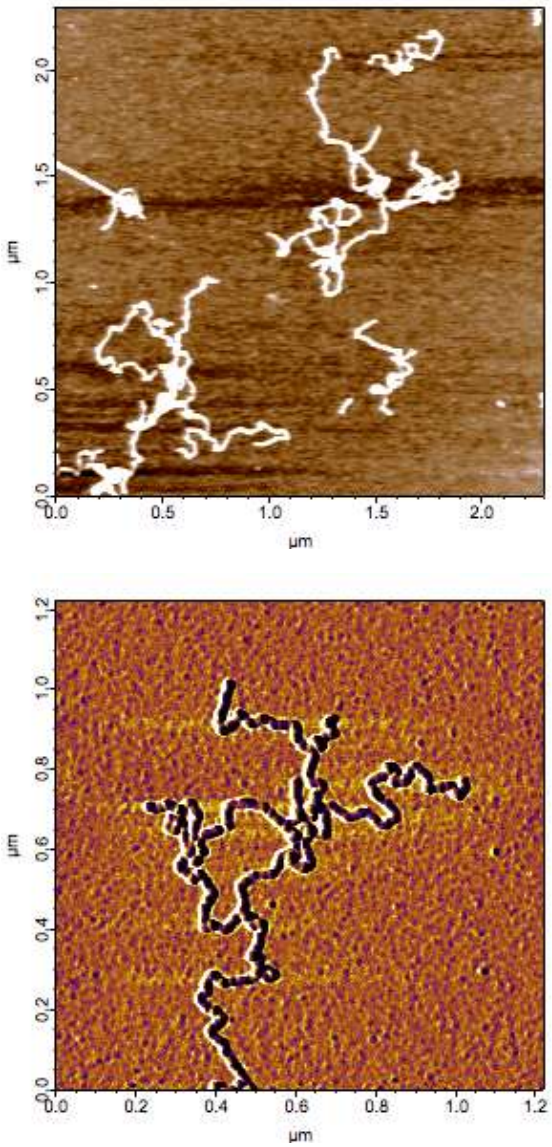

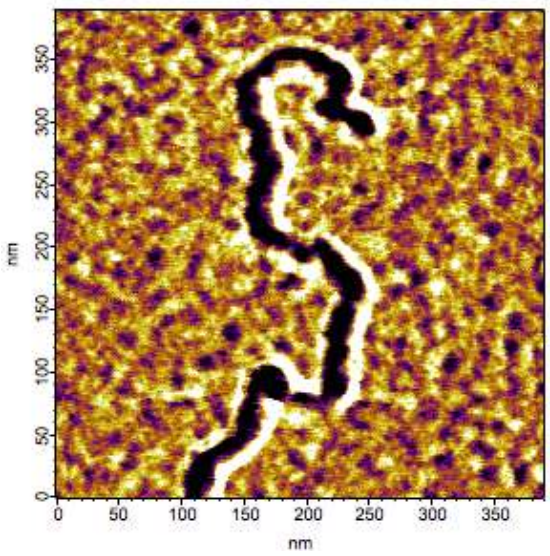
nm
0
50
100
150
200
250
300
350
nm